LUND UNIVERSITY

Nanomechanical phenotype of chondroadherin-null murine articular cartilage.

Batista, Michael A; Nia, Hadi T; Önnerfjord, Patrik; Cox, Karen A; Ortiz, Christine; Grodzinsky, Alan; Heinegård, Dick; Han, Lin

Link to publication

CrossMark

Brief report

Nanomechanical phenotype of chondroadherin-null murine articular cartilage

Michael A. Batista [a], Hadi T. Nia [b], Patrik Önnerfjord [c], Karen A. Cox [d], Christine Ortiz [a], Alan J. Grodzinsky [b,e,f], Dick Heinegård [c], Lin Han [a,g,*]

[a] Department of Materials Science and Engineering, Massachusetts Institute of Technology, Cambridge, MA 02139, United States
[b] Department of Mechanical Engineering, Massachusetts Institute of Technology, Cambridge, MA 02139, United States
[c] Department of Clinical Sciences, Lund University, 22184 Lund, Sweden
[d] Department of Developmental Biology, Harvard School of Dental Medicine, Boston, MA 02115, United States
[e] Department of Biological Engineering, Massachusetts Institute of Technology, Cambridge, MA 02139, United States
[f] Department of Electrical Engineering and Computer Science, Massachusetts Institute of Technology, Cambridge, MA 02139, United States
[g] School of Biomedical Engineering, Science and Health Systems, Drexel University, Philadelphia, PA 19104, United States

ARTICLE INFO

ABSTRACT

Chondroadherin (CHAD), a class IV small leucine rich proteoglycan/protein (SLRP), was hypothesized to play important roles in regulating chondrocyte signaling and cartilage homeostasis. However, its roles in cartilage development and function are not well understood, and no major osteoarthritis-like phenotype was found in the murine model with CHAD genetically deleted ($CHAD^{-/-}$). In this study, we used atomic force microscopy (AFM)-based nanoindentation to quantify the effects of CHAD deletion on changes in the biomechanical function of murine cartilage. In comparison to wild-type (WT) mice, CHAD-deletion resulted in a significant ≈ 70–80% reduction in the indentation modulus, E_{ind}, of the superficial zone knee cartilage of 11 weeks, 4 months and 1 year old animals. This mechanical phenotype correlates well with observed increases in the heterogeneity collagen fibril diameters in the surface zone. The results suggest that CHAD mainly plays a major role in regulating the formation of the collagen fibrillar network during the early skeletal development. In contrast, CHAD-deletion had no appreciable effects on the indentation mechanics of middle/deep zone cartilage, likely due to the dominating role of aggrecan in the middle/deep zone. The presence of significant rate dependence of the indentation stiffness in both WT and $CHAD^{-/-}$ knee cartilage suggested the importance of both fluid flow induced poroelasticity and intrinsic viscoelasticity in murine cartilage biomechanical properties. Furthermore, the marked differences in the nanomechanical behavior of WT versus $CHAD^{-/-}$ cartilage contrasted sharply with the relative absence of overt differences in histological appearance. These observations highlight the sensitivity of nanomechanical tools in evaluating structural and mechanical phenotypes in transgenic mice.

1. Introduction

The mechanical function of articular cartilage is determined by its extracellular matrix (ECM). Cartilage ECM is mainly composed of highly negatively charged aggrecan proteoglycans enmeshed within the type II/IX/XI heteropolymeric collagen (Eyre et al., 2006) fibrillar network (Maroudas, 1979; Han et al., 2011b). Proper assembly and organization of this ECM *in vivo* are regulated by a variety of secondary matrix proteins and proteoglycans, including collagen VI, thrombospondins, small leucine rich proteoglycans/proteins (SLRPs) and matrilins

(Heinegård, 2009). Despite their low concentrations in native cartilage, several of these molecules directly bind to the chondrocyte cell surface receptors to govern cell signaling, and others form important networks within the pericellular matrix. They can also bind pro-collagen molecules and, in many cases, remain bound to the newly formed fibers to provide additional stability and connectivity to other structural networks (Heinegård, 2009; Kalamajski and Oldberg, 2010; Iozzo et al., 2011).

Our study focuses on the roles of one particular regulatory molecule, chondroadherin (CHAD) (Larsson et al., 1991), a non-canonical class IV SLRP (Schaefer and Iozzo, 2008). CHAD is a 38 kD protein with 11 leucine-rich repeats (LRR) (Neame et al., 1994). It is localized within the epiphyseal growth plate during skeletal development and in the pericellular and territorial matrices in mature cartilage (Shen et al., 1998). In cartilage, CHAD mediates signaling between chondrocytes

* Corresponding author at: School of Biomedical Engineering, Science and Health Systems, Drexel University, Philadelphia, PA 19104, United States. Tel.: +1 215 571 3821; fax: +1 215 895 4983.
E-mail address: lh535@drexel.edu (L. Han).

and the ECM through binding to the α2β1 integrin (Camper et al., 1997; Haglund et al., 2011) and to cell surface proteoglycans such as syndecans (Haglund et al., 2013) (Fig. 1). CHAD also binds type II collagen and interacts with both the N- and C-terminal globular domains of type VI collagen (Camper et al., 1997; Månsson et al., 2001). It has thus been hypothesized that CHAD plays a critical role in regulating linkages between collagens and other ECM molecules *in vivo*, as well as the communication between chondrocytes and their surrounding matrices. Recently, gross histological and protein compositional analyses of CHAD-null murine joints have provided evidences that genetic deletion of CHAD can result in a distinct skeletal phenotype characterized by alterations in trabecular and cortical bone, widening of the epiphyseal growth plate, and variation in the molecular composition of cartilage, though no major osteoarthritis-like phenotype was found (Hessle et al., 2013). However, there is still a lack of understanding of whether deletion of the CHAD gene affects the biomechanical properties of articular cartilage, which are essential to the proper joint tissue function. Such changes in biomechanical properties may in the long term be linked to the initiation and progression of osteoarthritis.

In this study, we applied atomic force microscopy (AFM)-based nanoindentation to directly quantify the nanomechanical phenotype of CHAD-null murine articular cartilage. We assessed and compared the local biomechanical and collagen nanostructural properties of CHAD-null ($CHAD^{-/-}$) and wild-type (WT) murine knee cartilage in different depth-dependent zones (superficial and middle/deep zones) and at different ages. We found that the absence of CHAD significantly changed the collagen network assembly and mechanical properties of the superficial zone cartilage. These findings support the hypothesis that CHAD plays a critical role in the proper organization and function of cartilage ECM. In contrast, no differences in middle/deep zone cartilage were found. This study provides an important mechanics-based insight into how quantitatively minor ECM molecules, such as CHAD, may affect the biophysical functioning of cartilage otherwise thought to be dominated by collagens and aggrecan.

2. Results

AFM-based nanoindentation measures the indentation force, F, as a function of depth into the tissue, D, as the microspherical tip indents into the tested sample (i.e., cartilage) at a given rate (μm/s) (Fig. 2a). The F–D indentation curves were fit to the linear elastic Hertz model to account for the spherical indentation geometry and calculate the

Fig. 1. Schematic of the roles of chondroadherin in mediating chondrocyte signaling through bindings to the α2β1 integrin (Camper et al., 1997; Haglund et al., 2011) and surface proteoglycan syndecans (Haglund et al., 2013).

effective indentation modulus, E_{ind}. The values of E_{ind} thus depict the effective resistance of cartilage to indentation at the measured rate. For both $CHAD^{-/-}$ and WT cartilage, the F–D data were fit well by the predictions of the Hertz model (e.g., Fig. 2a, with least squares linear regression giving $R^2 > 0.96$). For each mouse type and age group, significant variation in E_{ind} was found between different mice within the same cohort (Kruskal–Wallis test, $p < 0.05$, Fig. 2b). In addition, heterogeneity in E_{ind} was also found between different locations on the same joint. All these variations are likely associated with differences in proteoglycan content and local collagen cross-link density within and between different joints given the known heterogeneous nature of cartilage (Hunziker et al., 2007; Han et al., 2011b). From each mouse, there was no significant difference between the E_{ind} measured on cartilage from left versus right knee (Fig. S1). Therefore, the average value of E_{ind} for the indents on cartilage of both knees from the same mouse was used to compare the effects of age and CHAD deletion (Fig. 3).

For all tested age groups, CHAD deletion resulted in a significant ≈ 70–80% reduction in E_{ind} of the superficial layer cartilage at all tested rates ($p < 0.0001$, two-way ANOVA on the global rank transforms) (Conover and Iman, 1981) (Fig. 3). This effect was even more prominent at the faster rate and younger ages (Fig. 3). This biomechanical difference correlates well with greater heterogeneity in the type II collagen-dominated fibril diameter distribution (F-test, $p < 0.0001$) observed on $CHAD^{-/-}$ mice at both 11 week and 4 month age groups measured via SEM (Fig. 4). In comparison to the distinctive nanomechanical phenotype in the superficial layer, no significant effect of CHAD deletion was found on the E_{ind} of the middle/deep zone cartilage cross-section at all tested rates ($p > 0.05$, two-way ANOVA on the global rank transforms) (Conover and Iman, 1981) (Fig. S2). In addition, significant indentation rate dependence was observed for both WT and $CHAD^{-/-}$ mice (Friedman's test, $p < 0.05$, Figs. 3, S3). Interestingly, in contrast to the distinct biomechanical phenotype of $CHAD^{-/-}$ mice measured by AFM nanoindentation, histological analysis did not yield any appreciable differences between WT and $CHAD^{-/-}$ mice with respect to the gross-level morphology and toluidine blue proteoglycan staining (Fig. 5).

3. Discussion

3.1. Roles of CHAD in murine cartilage mechanical properties

The weakening of cartilage upon CHAD deletion (Fig. 3) appears to be consistent with our hypothesis that CHAD has a biomechanically important function in the formation of an appropriately assembled fibrillar collagen network (Månsson et al., 2001) despite its low abundance (compared to collagen and aggrecan) and spatial localization within the territorial matrix (Shen et al., 1998). Lack of CHAD appears to slow down the development of the load bearing ECM, possibly due to alterations in both the chondrocyte cell signaling, as well as the assembly and linkages of the fibrillar collagen network. These effects could alter the cross-linking of the collagen network and, in turn, the local osmotic swelling and hydraulic permeability of the resident aggrecan. The fact that we observed increased heterogeneity in cartilage surface collagen fibrils (Fig. 4) further supports this statement. This effect is most salient in the cartilage superficial layer where the concentration of aggrecan is relatively low. Furthermore, the linkages between the collagen networks (types II and VI) and chondrocytes provided by CHAD (Camper et al., 1997; Haglund et al., 2011; Haglund et al., 2013) could have an effect of on the pericellular matrix. Indeed, in the superficial zone, a region with rather dense cell concentration (Stockwell, 1971), we detected significant differences in biomechanical properties (Fig. 3).

In comparison, we found CHAD deletion had no effects on the E_{ind} of the middle/deep zone cartilage (Fig. S2), where aggrecan concentration is substantially higher (Maroudas, 1979). Given the dominating role of aggrecan in cartilage middle/deep zone nanomechanics (Han et al., 2011a), the effects of changes in collagen fibril assembly on tissue
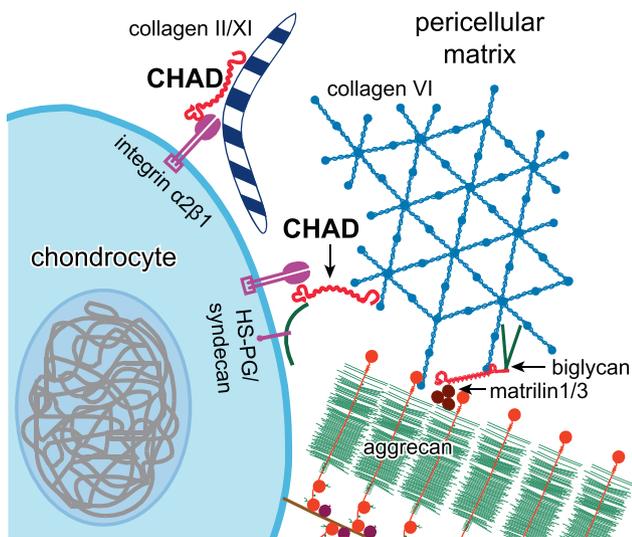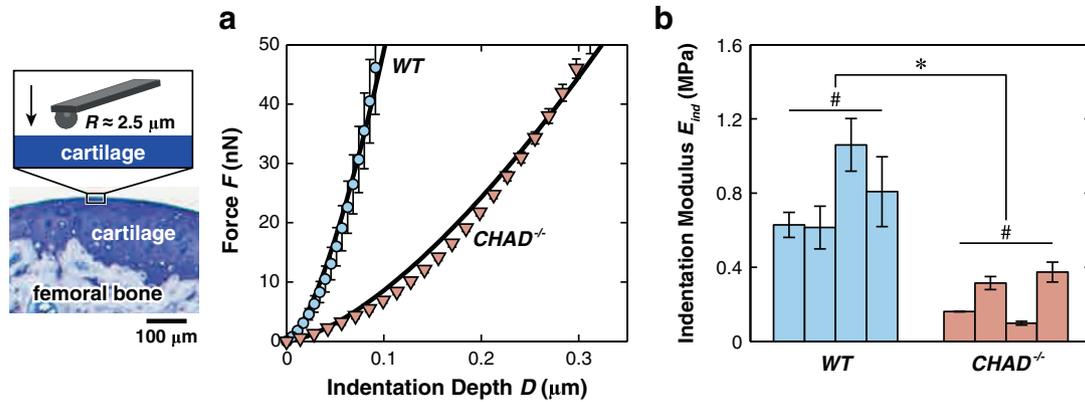
Fig. 2. (a) Typical indentation force versus depth loading curves (symbols) and corresponding Hertz model fit via least squares linear regression (solid lines, $R^2 > 0.96$). Data were obtained on the superficial layer of one right knee joint for 1 year old WT and $CHAD^{-/-}$ specimens. The density of experimental data was reduced to increase clarity. (b) Effective indentation modulus, E_{ind}, for 1 year old murine cartilage superficial layer from four animals in each mouse type (mean ± SEM of ≥ 8 locations on the same joint surface of each animal, *: $p < 0.05$ between WT and $CHAD^{-/-}$ via Mann–Whitney U test, #: $p < 0.05$ between different mice within each cohort of WT and $CHAD^{-/-}$ via Kruskal–Wallis test). Data shown were taken at 1 μm/s z-piezo displacement rate; the trends are the same for 0.1 and 10 μm/s rates.

biomechanics may not be as substantial as in the superficial layer. These regional effects of CHAD may seem contradictory to the known localization of CHAD in the middle/deep zone and its relative absence in the superficial zone of mature murine cartilage (Shen et al., 1998). However, immunostaining and mRNA expression also suggested the localization of CHAD in articular cartilage surface during the formation of cartilage (Shen et al., 1998). It is possible that CHAD plays an important regulatory role in determining the ECM assembly at the early stage of skeletal formation both in the growth plate and in the developing articular cartilage. Given the low turnover ratio of collagen (metabolic half life ≈ 117 years for human femoral head cartilage (Verzijl et al., 2000)), this effect could persist throughout skeletal development and aging up to one year in the mouse (Fig. 3). On the other hand, the absence of nanomechanical phenotype in the middle/deep zone suggests that it is likely that the effects of CHAD deletion on aggrecan concentration, an ECM constituent more rapidly turned over than collagen (aggrecan half life ≈ 3.4 years in human femoral head cartilage (Maroudas et al., 1998)), may be minimal. This scenario is supported by the fact that there are no substantial differences in histological staining of proteoglycans between WT and $CHAD^{-/-}$ cartilage (Fig. 5). However, at this point, we do not have quantitative information about the middle/deep zone collagen architecture or aggrecan concentration in $CHAD^{-/-}$ mice. Further characterization on $CHAD^{-/-}$ articular cartilage will help to better

elucidate the roles of CHAD in the structure–mechanics relationships of middle/deep zone cartilage.

While changes in the nanomechanics of $CHAD^{-/-}$ murine cartilage superficial layer can alter the joint contact mechanics, the impacts may not be strong enough to initiate pathological consequences of OA. Since $CHAD^{-/-}$ mice do not develop spontaneous OA, to further study the relevance of CHAD to OA (Hessle et al., 2013), $CHAD^{-/-}$ mice need to be combined with other induced OA models such as destabilization of the medial meniscus (DMM) (Glasson et al., 2007) or treadmill running (Li et al., 2010) models to compare its susceptibility to OA with the wild-type control.

3.2. Comparison to the roles of other SLRPs

This lack of OA phenotype in $CHAD^{-/-}$ mice is in marked contrast to the phenotype of other previously studied SLRP-deficient murine models. For example, biglycan-null ($Bgn^{-/0}$) (Ameye et al., 2002) and fibromodulin-null ($Fmd^{-/-}$) (Jepsen et al., 2002) mice both develop early OA. While the presence of OA in decorin-null ($Dcn^{-/-}$) mice was not confirmed, they were suggested to have joint laxity due to its weakened skin (Corsi et al., 2002). These differences are likely associated with the differences in both the molecular structures and localization of CHAD compared to other SLRPs. Firstly, while CHAD is a noncanonical class IV SLRP (Schaefer and Iozzo, 2008), it does not have a glycosaminoglycan (GAG) side chain like most other SLRPs (Neame et al., 1989). SLRPs with single GAG side chain, e.g., decorin and fibromodulin, regulate ECM fibrillogenesis and influence collagen cross-linking through bindings to type II pro-collagen and other molecules with both their LRR core proteins and the GAG chain (Hedbom and Heinegård, 1993). Biglycan, with two GAG side chains, has the highest efficiency in binding to type VI collagen to form hexagonal beads in the pericellular matrix (Wiberg et al., 2002). Without the GAG chain, the roles of CHAD in ECM assembly could be substantially different from other SLRPs although it is reported to bind to type II collagen as well (Månsson et al., 2001). Secondly, CHAD is mostly restricted in articular cartilage. In comparison, other SLRPs, such as decorin, biglycan and fibromodulin, are widely distributed across all other connective tissues up to maturity (Kalamajski and Oldberg, 2010). Therefore, while CHAD deletion results in distinctive bone phenotype mainly in the male mice, including higher bone mass density, altered cortical/trabecular bone thicknesses and increased structure bone index, no mechanical defects, such as reduced modulus or decreased fracture strength, were reported in the bone of $CHAD^{-/-}$ female mice (Hessle et al., 2013). OA is thus unlikely to arise from pre-disposed skeletal defects in $CHAD^{-/-}$ mice.
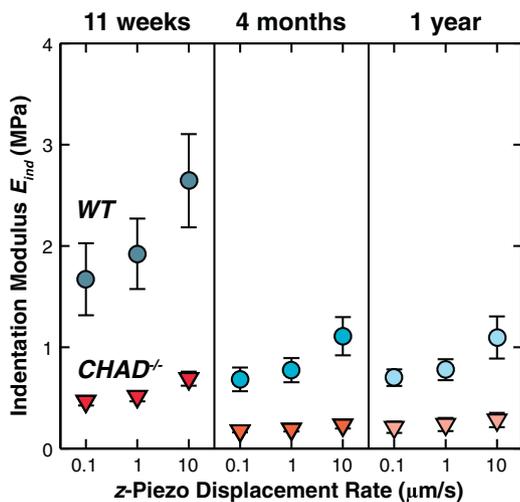
Fig. 3. Effective indentation modulus, E_{ind}, for WT and $CHAD^{-/-}$ murine cartilage superficial layer as a function of z-piezo displacement rate and mouse age (mean ± SEM of the average from each mouse, $n = 4$ animals for each model and age, except that $n = 5$ for WT at 4 months age).
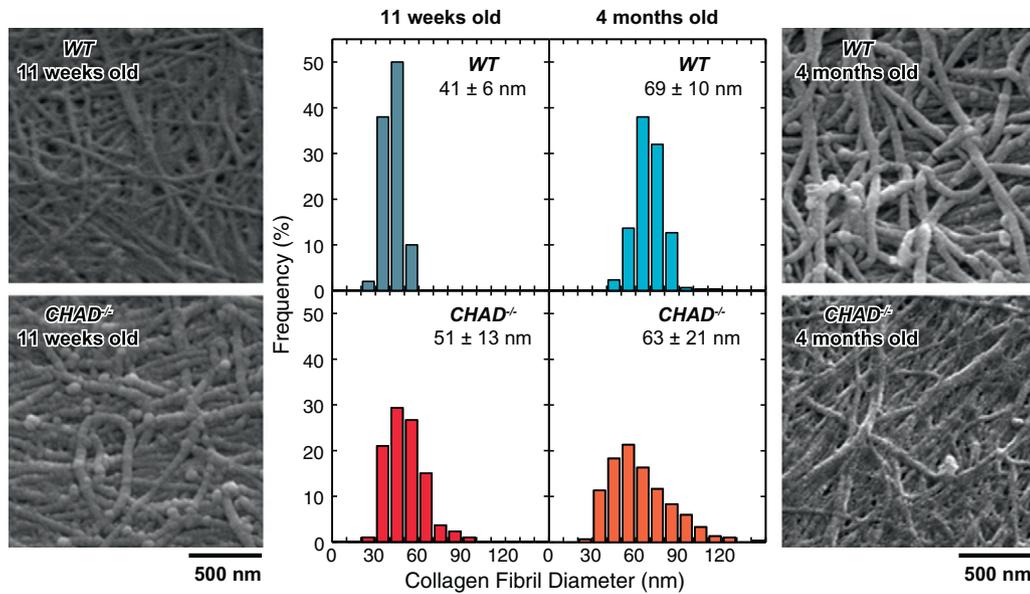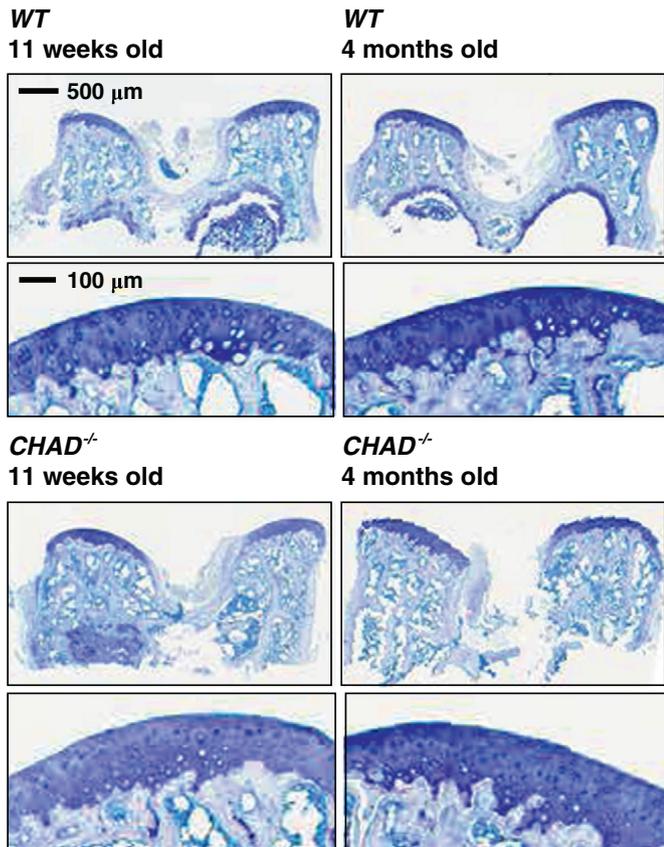
Fig. 4. Scanning electron microscope (SEM) images of *WT* and *CHAD*$^{-/-}$ murine cartilage surface prepared via the Ohtani's procedure (Ohtani, 1987) at 11 weeks and 4 months age, and corresponding histogram of collagen diameter distribution estimated on images from $n = 3$ animals (≥ 300 fibrils in total) for each model and age.

3.3. Rate-dependence of murine cartilage nanomechanics

The observed significant rate dependence (Fig. 3) is consistent with previous reports from both macroscopic tests (Hayes and Bodine, 1978; Mow et al., 1980; Grodzinsky et al., 1981) and micro/nanoindentation on cartilage from other species (Gupta et al., 2009; Miller and Morgan,

Fig. 5. Toluidine blue histology images of left knee joints from *WT* and *CHAD*$^{-/-}$ mice showing the absence of gross-level phenotype in *CHAD*$^{-/-}$ mice at 11 weeks and 4 months age.

2010; Han et al., 2011a). As the mechanical properties of cartilage ECM are directly governed by the hydrated type II/IX/XI collagen network and aggrecan, intrinsic macromolecular friction-governed viscoelasticity and fluid flow-dominated poroelasticity both contribute to the rate-dependence of E_{ind} (Han et al., 2011a). For *WT* mice, given the maximum indentation depth $D_{max} \approx 0.3$ μm, the deformation time during indentation is ≈ 60 ms (10 μm/s rate) to 6 s (0.1 μm/s rate). Similarly, for *CHAD*$^{-/-}$ mice, $D_{max} \approx 0.6$ μm, the deformation time is ≈ 120 ms to 12 s. Previous studies have shown that characteristic poroelastic relaxation time constant of cartilage is 10 to 100 ms at the μm-length scale (Han et al., 2011a; Nia et al., 2011). Poroelasticity is thus likely an important factor governing the measured rate dependence, especially at faster indentation rates (1 to 10 μm/s). In addition, intrinsic viscoelasticity of cartilage, due to matrix macromolecular friction, has a relaxation time constant ~10 s, independent of fluid flow length scales (June et al., 2009; Han et al., 2011a). It is another dominating mechanism, and is more important at slower rates (0.1 to 1 μm/s). Since deletion of CHAD did not have noticeable impact on the gross-level aggrecan staining (Fig. 5) and only altered the collagen network assembly (Fig. 4), these energy dissipative modes could be similar in *CHAD*$^{-/-}$ and *WT* mice. In fact, both *WT* and *CHAD*$^{-/-}$ cartilage superficial layer showed similar percentage of increase of E_{ind} from 0.1 μm/s to 1 μm/s ($\approx 10\%$) and 0.1 μm/s to 10 μm/s ($\approx 40 – 55\%$) rates (Mann–Whitney *U* test between *WT* and *CHAD*$^{-/-}$, $p > 0.05$, Fig. S3).

3.4. Advances and limitations of nanomechanical tools

Numerous transgenic and induced OA murine models have been used in cartilage and OA research owing to its low cost of maintenance and short life span (Ameye and Young, 2002, 2006). Murine model research of cartilage and OA mostly employed biochemical, gross-level histological and radiological assays to detect compositional and morphological phenotype. An important missing piece of knowledge is the biomechanical phenotype of cartilage, which is critical because the primary function of cartilage is mechanical. Given the relatively small size and irregular shape of murine cartilage compared to other species, AFM-based nanomechanical tools meet the needs of quantifying the mechanical properties of murine cartilage. Previously, AFM-based nanoindentation was used to detect the effects of maturation and OA-related degradation on the biomechanical properties of cartilage in type IX collagen-deleted mice (*Col9*$^{-/-}$) (Stolz et al., 2009). This study on

$CHAD^{-/-}$ mice further underlined AFM-nanoindentation as a viable tool in quantifying the spatially heterogeneous and rate-dependent nanomechanical phenotype in transgenic mice. Furthermore, since nanomechanical tools are measuring changes at much smaller length scales, they are more sensitive to detect matrix changes or OA-associated degradation than conventional microscopic assays such as histology or radiology. Further studies based on this paradigm will advance our knowledge of how other secondary ECM molecules, e.g., SLRPs, cartilage oligomeric matrix protein (COMP), matrilins, work synergistically to achieve a properly assembled and functioning cartilage matrix.

There are several limitations in the present study, in which advances in nanotechnology could elucidate more detailed nanomechanical and nanostructural phenotype to better understand the molecular origins of cartilage tissue function. The SEM imaging (Fig. 4) did not provide high enough resolution to reveal more detailed D-banding patterns or other sub-fibrillar level features of the collagen fibrils. Recent progression in helium ion microscopy (Vanden Berg-Foels et al., 2012) or tapping mode AFM imaging (Ng et al., 2003; Lee et al., 2013) could provide more details on the nanoscale structure of cartilage ECM molecules. In addition, AFM-based nanoindentation did not de-convolute the rate dependent mechanisms, i.e., fluid-flow induced poroelasticity and intrinsic viscoelasticity. Our recently developed custom-built AFM-nanorheometer (Nia et al., 2013) can be applied to murine cartilage to distinguish the effects of genetic modification on the viscoelastic and poroelastic energy dissipations that govern cartilage shock absorption during low frequency (e.g., walking) and high frequency (e.g., jumping, running) activities, respectively.

4. Conclusions

Using $CHAD^{-/-}$ murine model, we quantified the effects of CHAD deletion on the rate-dependent nanoindentation behaviors of articular cartilage in both the superficial and middle/deep zones at various ages. CHAD deletion resulted in significant reduction in E_{ind} of the superficial layer, which was accompanied by increased heterogeneity of the surface collagen fibril diameters. This effect is present in young mice at 11 weeks age, and persists during aging up to 1 year age. It is likely that deletion of CHAD affects collagen network assembly at the stage of early skeletal development, and this phenotype is manifested throughout the first year or more of the mouse life span. In comparison, the reduction of E_{ind} was absent in the middle/deep zone where aggrecan is more concentrated, suggesting less important impacts of CHAD in regulating the properties of aggrecan. As $CHAD^{-/-}$ cartilage shows no difference to the WT via histology, this contrast between nanomechanical and histological assays highlighted the high sensitivity of nanomechanical tools in evaluating the phenotype in transgenic murine articular cartilage.

5. Experimental procedures

5.1. Specimen generation

Chondroadherin-null mice ($CHAD^{-/-}$) were generated and confirmed via genotyping, as described previously (Hessle et al., 2013). Briefly, a linearized targeting vector was prepared with a phosphoglycerate kinase-neomycin resistance cassette (pGKNeo) enclosed between 3000 and 7000 bp CHAD gene fragments. Positive clones from semiconfluent R1 embryonic stem cells produced chimeric males. These males were crossed with B57BL/6 females. Males with a germ line transition were crossed to 129/sv females to produce the $CHAD^{-/-}$ mouse strain. $CHAD^{-/-}$ mice were backcrossed for ten generations into the C57BL/6 background before harvesting for nanomechanical tests.

5.2. Sample preparation

Female hind limbs from 11 weeks, 4 months, and 1 year old wild-type (WT) and $CHAD^{-/-}$ mice were disarticulated at the acetabulofemoral

(hip) joint following euthanasia, preserved in dry ice, and shipped overnight from Lund, Sweden to Cambridge, MA, USA. Joints were stored at −20 °C until dissection for <24 h in sterile phosphate buffered saline (PBS, without Mg^{2+}, Ca^{2+}) with protease inhibitors to minimize post-mortem degradation before indentation. After thawing at room temperature, joints were dissected to access the femoral lower extremity containing the intact femoral condyle articular cartilage surface. Femoral bone was cleaved above the femoral condyles after removal of tendon and ligament tissue. For nanoindentation of the superficial layer, dissected distal femurs were glued onto an AFM stainless steel disc. For nanoindentation of the middle/deep zone, dissected distal femurs were first sliced axially with a razor blade to reveal the inner cartilage tissue. Throughout the procedure, joints were maintained in PBS with protease inhibitors.

5.3. AFM-based nanoindentation

Atomic force microscopy (AFM)-based nanoindentation was performed using gold-coated silicon oxide spherical, colloidal probe tips (end radius $R \approx 2.5\ \mu m$, nominal spring constant $k \approx 4.5\ N/m$, Novascan, Ames, IA). Probe tips were functionalized with a neutral, hydroxyl-terminated self-assembled monolayer (OH-SAM) by immersion in 3 mM 11-mercaptoundecanol ($HS(CH_2)_{11}OH$) (Sigma-Aldrich) ethanol solution for 24 h. Calibration of cantilever deflection sensitivity (nm/V) was conducted on a hard mica surface in PBS and actual spring constants were determined via thermal oscillation method on a MFP-3D AFM (Asylum Research) (Hutter and Bechhoefer, 1993).

AFM-based nanoindentation was conducted on the medial femoral condyle of each joint in PBS to measure the effective indentation modulus of cartilage (Multimode AFM, Veeco, Santa Barbara, CA). Locally flat locations for nanoindentation were chosen by quantification of surface roughness via $5 \times 5\ \mu m$ AFM height image. Areas with surface roughness <~50 nm were selected for nanoindentation (Han et al., 2011a). At a given location, nanoindentation was conducted at constant z-piezo displacement rates of 0.1, 1 and 10 μm/s (approximately the indentation depth rates). For each joint, at least 8 different indentation locations were tested. For the joints from the same animals, data were pooled as no statistical differences were found between the joints from left versus right knees (Fig. S1). Nanoindentation was conducted on either the superficial zone cartilage (11 weeks, 4 months, 1 year age groups) or the top 10–50 μm, uncalcified middle/deep zone cartilage (11 weeks, 4 months age groups). For mouse cartilage, the middle zone only accounts for <20% of the total uncalcified cartilage thickness ($\approx 50\ \mu m$), and is indistinguishable from the deep zone (~60–80% of total thickness) (Hughes et al., 2005; Malda et al., 2013) under the AFM optical microscope. Optical microscope imaging of the specimen surface during experimentation verified that nanoindentation was conducted on unobstructed cartilage tissue.

From the indentation force versus depth curves obtained at each position and each rate, the Hertz model was applied to the loading (approach) portion to calculate the effective indentation modulus, E_{ind}, (Fig. 2a) after determining the effective tip-sample contact point using the Golden Section-based algorithm (Lin et al., 2007; Han et al., 2011a).

$$F = \frac{4}{3}\frac{E_{ind}}{(1-\nu^2)}R^{1/2}D^{3/2}, \tag{1}$$

where F is the indentation force, D is the indentation depth, R is the indentation tip radius ($R \approx 2.5\ \mu m$) and ν is the Poisson's ratio ($\nu = 0.1$ (Buschmann et al., 1999)). Since the mechanical properties of cartilage are time-dependent (Han et al., 2011a; Nia et al., 2011), E_{ind} does not represent the ideal elastic Young's modulus implied by Hertz model. Instead, E_{ind} is a non-equilibrium, rate-dependent parameter that can be used to compare the biomechanical impacts of CHAD deletion at various indentation rates. Nevertheless, the Hertz model appropriately accounts for the spherical indentation contact geometry (Timoshenko and Goodier, 1951).

5.4. Collagen fibril diameter and histology characterization

The nanoscale structure of the cartilage collagen network at 11 weeks and 4 months of age was characterized via scanning electron microscopy (Helios 600 Dual Beam FIB/SEM, FEI, Hillsboro, OR). These joints were fixed via the Ohtani's method to allow visualization of nanoscale fibrillar structures while maintaining the original shape and arrangement of collagen fibrils (Ohtani, 1987). Briefly, joints were fixed in 10% formalin for 1 day and stored in 10% NaOH for 6 days followed by Milli-Q filtered water rinsing for 1 day and a 5 hour immersion in 1–2% tannic acid. A second water rinse was followed by dehydration via an ascending alcohol series before counter-fixing in 1% OsO_4 for 2 h. Specimens were lyophilized (FreeZone Freeze-Dry System, Labconco, Kansas City, MO) and Au–Pd sputter coated (≈ 8 nm thickness) (Quorum Technologies, Guleph, Ontario, Canada) before imaging. Collagen fibril diameter and density was recorded from ≈ 300 collagen fibrils using SEM images (ImageJ) from WT and $CHAD^{-/-}$ cartilage surface (Fig. 4).

Histology with toluidine blue staining was conducted on the left side femoral condyles from 11 weeks and 4 months old WT and $CHAD^{-/-}$ mice to analyze gross level cartilage morphology (Geyer and Linss, 1978). The condyle was fixed in 10% glutaraldehyde overnight at 4 °C. The tissue was then decalcified, processed into paraffin and sectioned to 5 μm thick slices. The sections were mounted on glass slides. After removal of paraffin, the sections were rehydrated before staining with 1% toluidine blue working solution for 10 seconds to highlight the morphology and proteoglycan content in cartilage (Fig. 5). After staining, the slides were dehydrated and cover slipped, then photographed using the Zeiss AxioCam HRC digital camera attached to the Zeiss AxioImager M1 microscope.

5.5. Statistical tests

We used nonparametric statistical tests to avoid the assumption of normal distribution and homoscedasticity. The two-way analysis of variance (ANOVA) test on the global rank transforms, which is a nonparametric counterpart of two-way ANOVA (Conover and Iman, 1981), was performed to determine the effects of the CHAD deletion and age on the E_{ind} of both the superficial and middle-deep zones at each given rate. The Kruskal–Wallis test was performed to detect the variations between different animals within the same treatment group and age. The Friedman test was performed to examine the rate dependence of E_{ind}. In addition, the two-sample F-test was performed to determine if there was a statistically significant change in the variance of collagen fibril diameters between the WT and $CHAD^{-/-}$ mice. For each type of mice and each age, the diameters of collagen fibrils were measured on three mice. The data are pooled as no significant differences were found between the mice ($p > 0.05$ via Kruskal–Wallis test) for each type and age. In all tests, a p-value of less than 0.05 was taken as statistically significant.

Acknowledgments

Appendix A. Supplementary data

Supplementary data to this article can be found online at http://dx.doi.org/10.1016/j.matbio.2014.05.008.

References

Ameye, L., Young, M.F., 2002. Mice deficient in small leucine-rich proteoglycans: novel *in vivo* models for osteoporosis, osteoarthritis, Ehlers–Danlos syndrome, muscular dystrophy, and corneal diseases. Glycobiology 12, 107R–116R.

Ameye, L.G., Young, M.F., 2006. Animal models of osteoarthritis: lessons learned while seeking the 'Holy Grail'. Curr. Opin. Rheumatol. 18, 537–547.

Ameye, L., Aria, D., Jepsen, K., Oldberg, A., Xu, T., Young, M.F., 2002. Abnormal collagen fibrils in tendons of biglycan/fibromodulin-deficient mice lead to gait impairment, ectopic ossification, and osteoarthritis. FASEB J. 16, 673–680.

Buschmann, M.D., Kim, Y.-J., Wong, M., Frank, E., Hunziker, E.B., Grodzinsky, A.J., 1999. Stimulation of aggrecan synthesis in cartilage explants by cyclic loading is localized to regions of high interstitial fluid flow. Arch. Biochem. Biophys. 366, 1–7.

Camper, L., Heinegård, D., Lundgren-Åkerlund, E., 1997. Integrin α2β1 is a receptor for the cartilage matrix protein chondroadherin. J. Cell Biol. 138, 1159–1167.

Conover, W.J., Iman, R.L., 1981. Rank transformations as a bridge between parametric and nonparametric statistics. Am. Stat. 35, 124–129.

Corsi, A., Xu, T., Chen, X.-D., Boyde, A., Liang, J., Mankani, M., Sommer, B., Iozzo, R.V., Eichstetter, I., Robey, P.G., Bianco, P., Young, M.F., 2002. Phenotypic effects of biglycan deficiency are linked to collagen fibril abnormalities, are synergized by decorin deficiency, and mimic Ehlers–Danlos-like changes in bone and other connective tissues. J. Bone Miner. Res. 17, 1180–1189.

Eyre, D.R., Weis, M.A., Wu, J.-J., 2006. Articular cartilage collagen: an irreplaceable framework? Eur. Cell Mater. 12, 57–63.

Geyer, G., Linss, W., 1978. Toluidine blue staining of cartilage proteoglycan subunits. Acta Histochem. 61, 127–134.

Glasson, S.S., Blanchet, T.J., Morris, E.A., 2007. The surgical destabilization of the medial meniscus (DMM) model of osteoarthritis in the 129/SvEv mouse. Osteoarthritis Cartilage 15, 1061–1069.

Grodzinsky, A.J., Roth, V., Myers, E., Grossman, W.D., Mow, V.C., 1981. The significance of electromechanical and osmotic forces in the nonequilibrium swelling behavior of articular cartilage in tension. J. Biomech. Eng. 103, 221–231.

Gupta, S., Lin, J., Ashby, P., Pruitt, L., 2009. A fiber reinforced poroelastic model of nanoindentation of porcine costal cartilage: a combined experimental and finite element approach. J. Mech. Behav. Biomed. Mater. 2, 326–338.

Haglund, L., Tillgren, V., Addis, L., Wenglén, C., Recklies, A., Heinegård, D., 2011. Identification and characterization of the integrin α2β1 binding motif in chondroadherin mediating cell attachment. J. Biol. Chem. 286, 3925–3934.

Haglund, L., Tillgren, V., nnerfjord, P., Heinegård, D., 2013. The C-terminal peptide of chondroadherin modulates cellular activity by selectively binding to heparan sulfate chains. J. Biol. Chem. 288, 995–1008.

Han, L., Frank, E.H., Greene, J.J., Lee, H.-Y., Hung, H.-H.K., Grodzinsky, A.J., Ortiz, C., 2011a. Time-dependent nanomechanics of cartilage. Biophys. J. 100, 1846–1854.

Han, L., Grodzinsky, A.J., Ortiz, C., 2011b. Nanomechanics of the cartilage extracellular matrix. Annu. Rev. Mater. Res. 41, 133–168.

Hayes, W.C., Bodine, A.J., 1978. Flow-independent viscoelastic properties of articular cartilage matrix. J. Biomech. 11, 407–419.

Hedbom, E., Heinegård, D., 1993. Binding of fibromodulin and decorin to separate sites on fibrillar collagens. J. Biol. Chem. 268, 27307–27312.

Heinegård, D., 2009. Proteoglycans and more—from molecules to biology. Int. J. Exp. Pathol. 90, 575–586.

Hessle, L., Stordalen, G.A., Wenglén, C., Petzold, C., Tanner, K.E., Brorson, S.-H., Baekkevold, E.S., Önnerfjord, P., Reinholt, F.P., Heinegård, D., 2013. The skeletal phenotype of chondroadherin deficient mice. PLoS One 8, e63080.

Hughes, L.C., Archer, C.W., ap Gwynn, I., 2005. The ultrastructure of mouse articular cartilage: collagen orientation and implications for tissue functionality. A polarised light and scanning electron microscope study and review. Eur. Cell. Mater. 9, 68–84.

Hunziker, E.B., Kapfinger, E., Geiss, J., 2007. The structural architecture of adult mammalian articular cartilage evolves by a synchronized process of tissue resorption and neoformation during postnatal development. Osteoarthritis Cartilage 15, 403–413.

Hutter, J.L., Bechhoefer, J., 1993. Calibration of atomic-force microscope tips. Rev. Sci. Instrum. 64, 1868–1873.

Iozzo, R.V., Goldoni, S., Berendsen, A.D., Young, M.F., 2011. Small leucine-rich proteoglycans. In: Mecham, R.F. (Ed.), The Extracellular Matrix: An Overview. Springer-Verlag, Berlin, pp. 197–231.

Jepsen, K.J., Wu, F., Peragallo, J.H., Paul, J., Roberts, L., Ezura, Y., Oldberg, A., Birk, D.E., Chakravarti, S., 2002. A syndrome of joint laxity and impaired tendon integrity in lumican- and fibromodulin-deficient mice. J. Biol. Chem. 277, 35532–35540.

June, R.K., Ly, S., Fyhrie, D.P., 2009. Cartilage stress-relaxation proceeds slower at higher compressive strains. Arch. Biochem. Biophys. 483, 75–80.

Kalamajski, S., Oldberg, Å., 2010. The role of small leucine-rich proteoglycans in collagen fibrillogenesis. Matrix Biol. 29, 248–253.

Larsson, T., Sommarin, Y., Paulsson, M., Antonsson, P., Hedbom, E., Wendel, M., Heinegård, D., 1991. Cartilage matrix proteins. A basic 36-kda protein with a restricted distribution to cartilage and bone. J. Biol. Chem. 266, 20428–20433.

Lee, H.-Y., Han, L., Roughley, P.J., Grodzinsky, A.J., Ortiz, C., 2013. Age-related nanostructural and nanomechanical changes of individual human cartilage aggrecan monomers and their glycosaminoglycan side chains. J. Struct. Biol. 181, 264–273.

Li, J., Anemaet, W.K., Diaz, M.A., Buchanan, S., Tortorella, M., Malfait, A.M., Mikecz, K., Sandy, J.D., Plaas, A., 2010. Knockout of ADAMTS5 does not eliminate cartilage aggrecanase activity but abrogates joint fibrosis and promotes cartilage aggrecan deposition in murine osteoarthritis models. J. Orthop. Res. 29, 516–522.

Lin, D.C., Dimitriadis, E.K., Horkay, F., 2007. Robust strategies for automated AFM force curve analysis—I. Non-adhesive indentation of soft, inhomogeneous materials. J. Biomech. Eng. 129, 430–440.

Malda, J., de Grauw, J.C., Benders, K.E.M., Kik, M.J.L., van de Lest, C.H.A., Creemers, L.B., Dhert, W.J.A., van Weeren, P.R., 2013. Of mice, men and elephants: the relation between articular cartilage thickness and body mass. PLoS One 8, e57683.

Månsson, B., Wenglén, C., Mörgelin, M., Saxne, T., Heinegård, D., 2001. Association of chondroadherin with collagen type II. J. Biol. Chem. 276, 32883–32888.

Maroudas, A., 1979. Physicochemical properties of articular cartilage. In: Freeman, M.A.R. (Ed.), Adult Articular Cartilage. Pitman, England, pp. 215–290.

Maroudas, A., Bayliss, M.T., Uchitel-Kaushansky, N., Schneiderman, R., Gilav, E., 1998. Aggrecan turnover in human articular cartilage: use of aspartic acid racemization as a marker of molecular age. Arch. Biochem. Biophys. 350, 61–71.

Miller, G.J., Morgan, E.F., 2010. Use of microindentation to characterize the mechanical properties of articular cartilage: comparison of biphasic material properties across length scales. Osteoarthritis Cartilage 18, 1051–1057.

Mow, V.C., Kuei, S.C., Lai, W.M., Armstrong, C.G., 1980. Biphasic creep and stress relaxation of articular cartilage in compression: theory and experiments. J. Biomech. Eng. 102, 73–84.

Neame, P.J., Choi, H.U., Rosenberg, L.C., 1989. The primary structure of the core protein of the small, leucine-rich proteoglycan (PG I) from bovine articular cartilage. J. Biol. Chem. 264, 8653–8661.

Neame, P.J., Sommarin, Y., Boynton, R.E., Heinegård, D., 1994. The structure of a 38-kDa leucine-rich protein (chondroadherin) isolated from bovine cartilage. J. Biol. Chem. 269, 1–8.

Ng, L., Grodzinsky, A.J., Patwari, P., Sandy, J., Plaas, A., Ortiz, C., 2003. Individual cartilage aggrecan macromolecules and their constituent glycosaminoglycans visualized via atomic force microscopy. J. Struct. Biol. 143, 242–257.

Nia, H.T., Han, L., Li, Y., Ortiz, C., Grodzinsky, A.J., 2011. Poroelasticity of cartilage at the nanoscale. Biophys. J. 101, 2304–2313.

Nia, H.T., Bozchalooi, I.S., Li, Y., Han, L., Hung, H.-H., Frank, E.H., Youcef-Toumi, K., Ortiz, C., Grodzinsky, A.J., 2013. High-bandwidth AFM-based rheology reveals that cartilage is most sensitive to high loading rates at early stages of impairment. Biophys. J. 104, 1529–1537.

Ohtani, O., 1987. Three-dimensional organization of the connective tissue fibers of the human pancreas: a scanning electron microscopic study of NaOH treated-tissues. Arch. Histol. Jpn. 50, 557–566.

Schaefer, L., Iozzo, R.V., 2008. Biological functions of the small leucine-rich proteoglycans: from genetics to signal transduction. J. Biol. Chem. 283, 21305–21309.

Shen, Z.X., Gantcheva, S., Månsson, B., Heinegård, D., Sommarin, Y., 1998. Chondroadherin expression changes in skeletal development. Biochem. J. 330, 549–557.

Stockwell, R.A., 1971. The interrelationship of cell density and cartilage thickness in mammalian articular cartilage. J. Anat. 109, 411–421.

Stolz, M., Gottardi, R., Raiteri, R., Miot, S., Martin, I., Imer, R., Staufer, U., Raducanu, A., Düggelin, M., Baschong, W., Daniels, A.U., Friederich, N.F., Aszodi, A., Aebi, U., 2009. Early detection of aging cartilage and osteoarthritis in mice and patient samples using atomic force microscopy. Nat. Nanotechnol. 4, 186–192.

Timoshenko, S., Goodier, J.N., 1951. Thermal stress, Theory of Elasticity2nd ed. McGraw-Hill, New York, NY, pp. 399–437.

Vanden Berg-Foels, W.S., Scipioni, L., Huynh, C., Wen, X., 2012. Helium ion microscopy for high-resolution visualization of the articular cartilage collagen network. J. Microsc. 246, 168–176.

Verzijl, N., DeGroot, J., Thorpe, S.R., Bank, R.A., Shaw, J.N., Lyons, T.J., Bijlsma, J.W.J., Lafeber, F.P.J.G., Baynes, J.W., TeKoppele, J.M., 2000. Effect of collagen turnover on the accumulation of advanced glycation end products. J. Biol. Chem. 275, 39027–39031.

Wiberg, C., Heinegård, D., Wenglén, C., Timpl, R., Mörgelin, M., 2002. Biglycan organizes collagen VI into hexagonal-like networks resembling tissue structures. J. Biol. Chem. 277, 49120–49126.